Direct Observation of Different One- and Two-Photon Fluorescent States in a Pyrrolo[3,2-*b*]pyrrole Fluorophore

Yangzhong Qin,[a,¥] Christoph Schnedermann,[a,+,¥] Mariusz Tasior,[b] Daniel T. Gryko*,[b] and Daniel G. Nocera*,[a]

[a] *Department of Chemistry and Chemical Biology, Harvard University, Cambridge, MA 02138.* [b] *Institute of Organic Chemistry, Polish Academy of Sciences, Kasprzaka 44/52, 01-224 Warsaw, Poland*

ABSTRACT: Two-photon fluorophores are frequently employed to obtain superior spatial resolution in optical microscopy applications. To guide the rational design of these molecules, a detailed understanding of their excited-state deactivation pathways after two-photon excitation is beneficial, especially to assess the often-assumed presumption that the one- and two-photon excited-state dynamics are similar after excitation. Here, we showcase the breakdown of this assumption for one- and two-photon excitation of a centrosymmetric pyrrolo[3,2-*b*]pyrrole chromophore by combining time-resolved fluorescence and broadband femtosecond transient absorption spectroscopy. Compared to one-photon excitation, where radiative decay dominates the photodynamics, two-photon excitation leads to dynamics arising from increased non-radiative decay pathways. These different photodynamics are manifest to different quantum yields, thus highlighting the types of time-resolved studies described here to be valuable guideposts in the design of two-photon fluorophores for imaging applications.

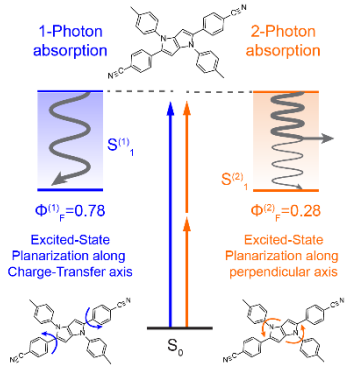

Two-photon absorbing (2PA) fluorophores are consequential imaging reagents in biology and life science applications as they facilitate enhanced three-dimensional spatial resolution and offer deeper penetration depths compared to their one-photon absorption (1PA) analogues.[1-4] Further advantages of 2PA fluorescent imaging techniques lie in a reduced phototoxicity, background fluorescence, and attenuated sample degradation attendant to longer wavelength excitation, all of which improves the image quality.[4-7] Beyond imaging applications, 2PA chromophores offer a range of desirable optical properties suitable for optical memory storage[8-10] as well as photodynamic therapy.[11-14]

Extensive research has been carried out in exploring design principles of 2PA molecules and optimizing 2PA cross sections.[15-17] A promising molecular platform, which offers versatility and tunability in 2PA fluorescence, is based on an electron donating (D) pyrrolo[3,2-*b*]pyrrole core catenated with diametrically opposing phenyl groups possessing electron accepting substituents (A).The 2,5-bis(4-cyanophenyl)-1,4-bis(4-methylphenyl)-1,4-dihydro-pyrrolo[3,2-*b*]pyrrole **ADA** shown in Scheme 1 is an example of this class of centrosymmetric, quadrupolar molecules.[18-22] These acceptor-donor-acceptor fluorophores display high 2PA cross-sections, on the order of 10^2–10^3 GM.[23,24] Minor changes in its 1PA spectrum over a wide range of solvents have led **ADA** to be identified as a quadrupolar molecule.[24] Compelling evidence has been provided that **ADA** undergoes rapid excited-state symmetry breaking following 1PA to form a dipolar fluorescent state,[25-27] whereby the associated photodynamics are intimately connected to the solvent environment.[27-29]

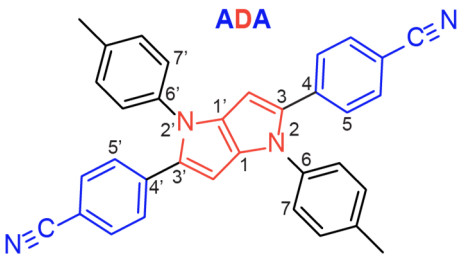

Scheme 1. Molecular structure of 2,5-bis(4-cyanophenyl)-1,4-bis(4-methylphenyl)-1,4-dihydropyrrolo[3,2-*b*]pyrrole **ADA**. Number convention is shown in grey for important atoms.

Whereas **ADA** has been studied systematically after 1PA for a range of experimental conditions,[23-26,28] investigation of its excited-states and dynamics following 2PA has eluded characterization. To address this shortcoming, we combine time-resolved fluorescence and broadband femtosecond transient absorption spectroscopy with quantum chemical calculations to elucidate the excited-state deactivation pathways following 1PA and 2PA in **ADA** (Scheme 1). Although the fluorescent excited-state is populated in <150 fs after photoexcitation with either type of excitation, our results suggest that the properties of the fluorescent state accessed after 2PA differs from the corresponding 1PA state, both in spectral shape and lifetime. Following 2PA excitation, non-radiative decay channels dominate the excited-state dynamics resulting in a reduced fluorescence quantum yield as compared to that measured for 1PA

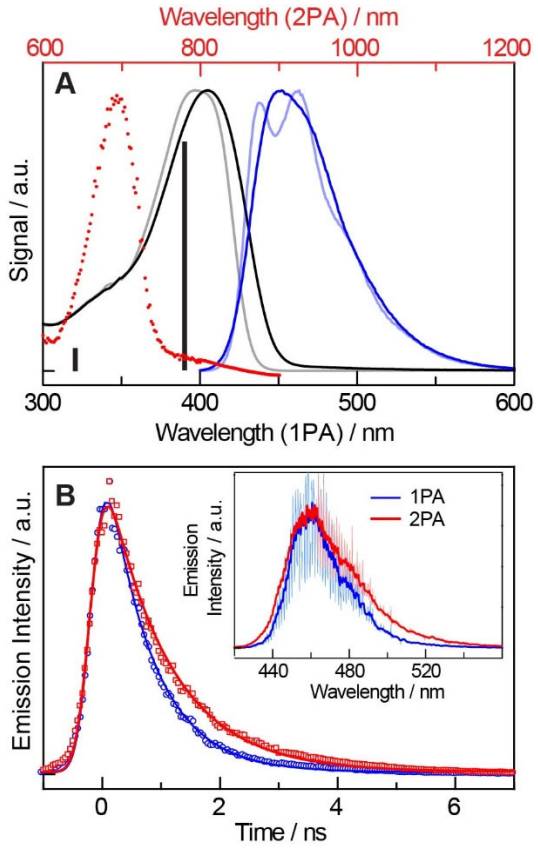

Figure 1. A 1PA (black line) and corresponding fluorescence (blue line) spectra of **ADA** in dichloromethane (DCM) and cyclohexane (CHX) (grey and powder blue lines for 1PA and fluorescence, respectively) after photoexcitation at 360 nm. The 2PA spectrum (red dotted line) is also shown and has been reprinted with permission from ref. 24. The top horizontal axis (red) refers to the employed laser wavelength for 2PA measurements. Calculated electronic 1PA transitions in DCM are indicated by black sticks. **B** Time-resolved fluorescence decay integrated from 440 to 520 nm of **ADA** in DCM after 1PA (360 nm, blue trace) and 2PA (720 nm, red trace). Solid lines indicate single-exponential model fittings with a lifetime of 770 ps for 1PA (blue line) and 1050 ps for 2PA (red line, see the SI for details). The time-integrated fluorescence spectrum is shown in the inset. The raw data (opaque) is also shown and was smoothed by 5-point moving average. The small red-shift of the fluorescence spectrum compared to the steady-state fluorescence spectrum in Figure 1A is due to calibration differences but does not affect our comparison (see experimental methods in supporting information).

excitation. A consequence of the different nonradiative decay channels arising from 1PA and 2PA excitation is that 2PA cross-sections for **ADA** have been underestimated. Such a discrepancy between 1PA and 2PA is important to quantify as the need for accurate cross-sections is crucial to a variety of quantitative imaging applications, such as metabolic imaging of tumors.[30,31] The studies reported herein provide a general methodology to investigate the excited-state photodynamics after two- or multi-photon excitation,[32-34] and hence better characterize the optical properties of 2PA fluorophores for optimized performance and quantification of 2PA imaging.

The 1PA spectrum of **ADA** is characterized by features at 404 and 330 nm in dichloromethane (DCM, black line in Figure 1A) and 398 and 330 nm in cyclohexane (CHX, grey line in Figure 1A). Time-dependent density-functional theory calculations (TD-DFT, black stick spectrum in Figure 1A) leads us to assign these 1PA allowed transitions to S_1 and S_2. The corresponding peak at 346 nm (red dotted line in Figure 1A) in the 2PA spectrum is assigned to the lowest 2PA allowed transition to S_3. This assignment is consistent with previous computations on similar, centrosymmetric acceptor-donor-acceptor molecules, but we note that the choice of functional can interchange the energetic ordering of S_2 and S_3 states due to their energetic proximity (Figure 1A, compare 1PA and 2PA spectra).[24] In the approximate C_2 point group of **ADA**, the S_0 electronic ground state can be assigned to A symmetry and the corresponding S_1 and S_2 excited-states are of B symmetry. The S_3 excited-state is of A symmetry, as expected from the selection rules.

The 1PA fluorescence spectrum of **ADA** in DCM (Figure 1A, blue line) peaks at 450 nm and is featureless, whereas the fluorescence spectrum in CHX (Figure 1A, light blue line) displays a vibronic progression with peaks/shoulders at 438, 464, 493, 526 nm corresponding to an average frequency difference of 1274 cm^{-1} (see Figure S1A). In the non-polar solvent environment of CHX, solvent-solute interactions are minimized thus leading to better defined vibronic structure. This observation is consistent with the calculated partial planarization of **ADA** from an initial 4-cyanophenyl/pyrrolo-pyrrole core dihedral angle ($\angle N_2$–C_3–C_4–C_5 and $\angle N_{2'}$–$C_{3'}$–$C_{4'}$–$C_{5'}$) of –32.5° to –19.4° in the relaxed S_1 state (see Scheme 1 for numbering convention and optimized structure files provided in the SI). In the polar DCM solvent, solvent-solute coupling broadens the involved transitions, resulting in a loss of vibronic fine structure. Similar observations have been reported for structurally-related substituted biphenyls.[35]

Heretofore, the 2PA fluorescence spectrum has not been reported for **ADA**. To examine the spectrum and the dynamics of the fluorescent state after 2PA, we conducted time-resolved fluorescence spectroscopy at an excitation wavelength of 720 nm and compared the results with iso-energetic 1PA excitation at 360 nm for the molecule in DCM (Figure 1B). The corresponding fluorescence spectrum peaks at 460 nm for both excitation wavelengths but is accompanied by spectral broadening for 2PA (Figure 1B, inset). In addition, whereas 1PA engenders mono-exponential decay dynamics with a time constant of 770 ps (Figure 1, blue trace), 2PA gives rise to an attenuated fluorescence decay of 1050 ps (Figure 1, red trace). Similar results were obtained in CHX (Figure S1B) and we therefore restrict our discussions to DCM. The absorbance of samples at the 360 nm excitation wavelength in CHX and DCM are 0.11 and 0.28, respectively. Thus observed differences in the emission spectra and decays under 1PA and 2PA are not perturbed by self-absorption (see SI and Figure S2). Although the broadening in the 2PA fluorescent spectrum is modest as compared to that obtained from 1PA excitation, the prolonged lifetime of the former is significant. These results provide compelling evidence that 2PA accesses a different fluorescent state. Our experimental results suggest that the fluorescent state following 2PA has the same electronic character as the 1PA fluorescent S_1 state, as evidenced by the same fluorescence maximum wavelength but falls on a different part of the potential energy surface most likely due to a different, more flexible configuration indicated by the broadened fluorescence spectrum (vide infra). The different nature of the fluorescent 2PA state is of consequence to the previously reported 2PA cross-section,

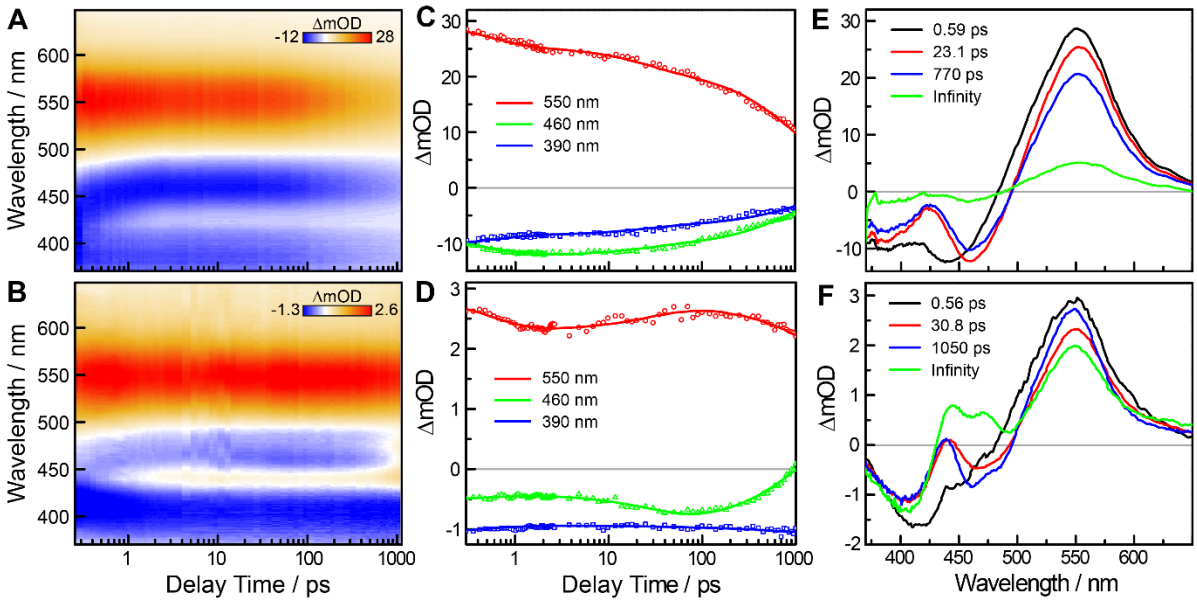

Figure 2. Broadband femtosecond transient absorption spectra of **ADA** in DCM after **A** 1PA at 360 nm and **B** 2PA at 720 nm. Temporal evolution of representative transients characterizing the ESA (550 nm, red), SE (460 nm, green) and GSB (390 nm, blue) for **ADA** after **C** 1PA and **D** 2PA. Solid lines show a global fit (A → B → C → D → model). Retrieved evolution-assisted decay spectra from global fitting for **E** 1PA and **F** 2PA. Associated time constants are indicated in the legend. Infinity stands for a time constant far beyond the setup detection range.

which was previously obtained using two-photon fluorescence excitation (TPFE) spectroscopy.[36,37] In deriving the relevant cross-section, it is typically assumed that the fluorescent states between 1PA and 2PA are identical and that the corresponding fluorescence quantum yields are also the same. Our results suggest that this is not the case for **ADA**. Although the difficulty associated with a direct measure of the absolute 2PA fluorescence quantum yield has been noted,[36,37] we set out to quantify the 2PA fluorescence quantum yield relative to 1PA by performing broadband femtosecond transient absorption spectroscopy. This method allows us to directly follow the excited-states with femtosecond time resolution for both 1PA and 2PA excitation conditions and thus estimate the relative 2PA fluorescence quantum yield.

The transient absorption dynamics for **ADA** in DCM after 1PA (360 nm) and 2PA (720 nm) are shown in Figures 2A and 2B, respectively (and in Figure S3 for **ADA** in CHX). The spectra show three distinct spectral features after photoexcitation: (1) a positive signal centered at 550 nm indicating excited-state absorption (ESA), (2) a negative signal at 460 nm predominantly corresponding to stimulated emission (SE) and (3) a negative signal below 425 nm (Figure 2A) and 440 nm (Figure 2B), corresponding to the ground-state bleach (GSB). For the 1PA transient absorption dynamics presented in Figure 2A, the SE maximum matches the peak of the fluorescence spectrum (Figure 1) and we observe a clear Stokes shift due to vibrational cooling and solvent relaxation (also observed in 2PA spectrum, *vide infra*).[38-42] Previous report has shown a fluorescence quantum yield of 0.78 for **ADA** dissolved in DCM after 1PA.[18] The large fluorescence quantum yield indicates that the major decay pathway is radiative; the non-radiative component is partitioned between decay to ground state and to a triplet state, as evidenced by a long-lived transient signal observed in nanosecond transient absorption measurements, that decays over 1 μs (Figure S4). The 1PA transient absorption results are in excellent agreement with previous studies.[25]

Despite the similar transient absorption spectral profiles under 1PA and 2PA excitation, we clearly find different excited-state decay dynamics, particularly from 30 ps to 1 ns (Figures 2C and 2D show representative dynamics of the individual spectral features). Following 1PA, the three components (GSB, SE and ESA) decay within 1 ns by 64.2%, 65.7% and 63.7%, respectively; this result is in line with the fluorescence decay lifetime of 770 ps (based on this lifetime, the decay of the excited-state should be 72.7% at 1 ns). This concerted decay behavior suggests that the 1PA excited-state dynamics on this timescale are dominated by radiative decay to the ground state with minor contributions from non-radiative decay channels. More complicated excited-state dynamics are observed after 2PA. The 2PA SE signal decay (Figure 2D, green line) is markedly different than that of the GSB recovery (Figure 2D, blue line) and ESA decay (Figure 2D, red line). The SE signal at 460 nm initially increases in intensity over 100 ps, most likely due to vibrational cooling and solvent relaxation, after which it decreases at an apparent rate that is faster than the 2PA fluorescence lifetime of 1050 ps. As the SE and fluorescence decay should conform in the simplest scenario, the accelerated apparent decay suggests that there are two processes being recorded at 460 nm—SE decay signal over 1050 ns overlaid with the growth of an ESA signal. Surprisingly, the ESA (at 550 nm) and GSB (at 390 nm) signals change within 1 ns by only 14.8% and 11.8%, respectively. The small amplitude changes in ESA and GSB over this timescale suggests that the fluorescent state does not relax to the ground state as observed for 1PA, but decays to a longer-lived (>1 ns) excited-state, which is also consistent with the formation of a triplet state in correspondence to

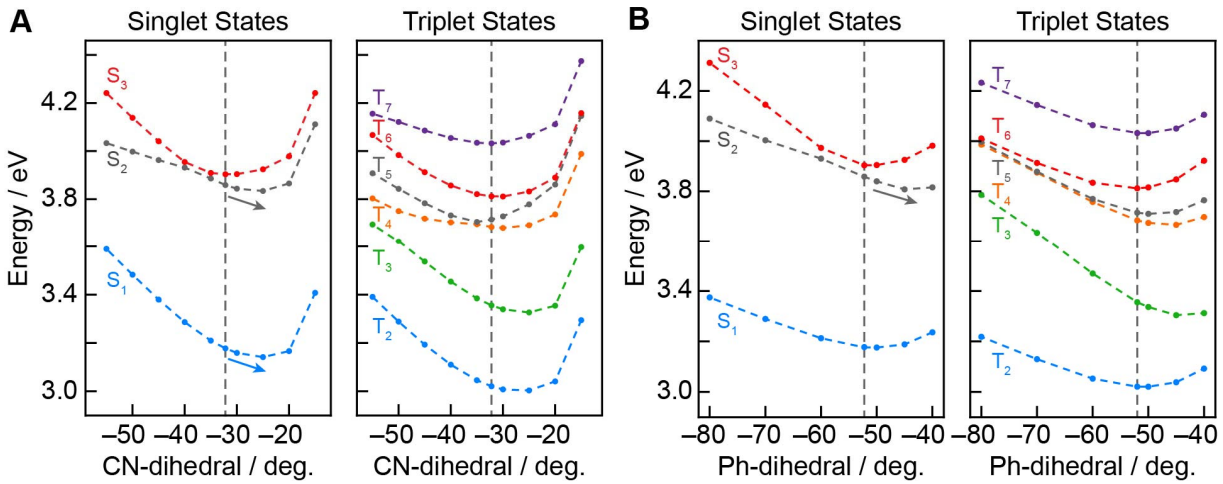

Figure 3. Energy levels of **ADA** as a function of the **A** cyanophenyl pyrrolo-pyrrole and **B** phenyl pyrrolo-pyrrole dihedral angle. Singlet state (left) and triplet state (right) energies are obtained at the MN15/def2-TZVP, cPCM (DCM) level of theory by concertedly adjusting both dihedral angles (∠N_2-C_3-C_4-C_4 and ∠$N_{2'}$-$C_{3'}$-$C_{4'}$-$C_{5'}$ for the CN-dihedral or ∠C_1-N_2-C_6-C_7 and ∠$C_{1'}$-$N_{2'}$-$C_{6'}$-$C_{7'}$ for the Ph-dihedral). The remaining degrees of freedom were taken from the optimized ground-state structure (see supporting information for further discussion and Scheme 1 for numbering convention). The dashed grey vertical lines indicate the ground-state equilibrium value of the corresponding dihedral angle and solid arrows in the singlet plots indicate important potential energy surface gradients.

our observations for 1PA dynamics. While we are unable to directly measure 2PA nanosecond transient absorption spectra, we can rationalize a triplet state assignment based on a TA signal extending beyond 1 ns (not shown) and the results of quantum computations (see below).

To extract the kinetics and spectral details underlying the broadband transient absorption response (Figures 2A and 2B) we globally fitted the data to a serial model (A→B→C→D→).[43] The fitted data from this serial model at the selected wavelengths of the ESA, GSB and SE spectra are highlighted by the solid lines in Figures 2C and 2D. Following 1PA, the excited-state rapidly decays in 0.59 ps (Figure 2E, black) due to vibrational cooling. Subsequently, we find a slower decay component of 23.1 ps (Figure 2E, red) due to solvent relaxation followed by a component of 770 ps (Figure 2E, blue) to form a triplet state that persists beyond our probed time window (Figure 2E, green). We fixed the longest decay constant during our fitting to 770 ps as determined by the excited-state lifetime measured via time-resolved fluorescence (Figure 1B). The 2PA transient absorption response was described in the same way (Figures 2D and 2F) by fixing the longest decay constant to 1050 ps (Figure 2F, blue), determined by 2PA fluorescence lifetime (Figure 1B). The two fast components of 0.56 ps and 30.8 ps (Figure 2F, black and red) match their corresponding 1PA values, further supporting our assignment to vibrational cooling and solvent relaxation, respectively. Consistent with the observation of different decay kinetics (Figure 2C and 2D) of 1PA and 2PA, the major difference shown by the EADS for the **ADA** in DCM is the signal drop from fully relaxed excited-state (blue lines in Figures 2E and 2F) to the long-lived triplet state (green lines in Figures 2E and 2F): while the ESA signal at 550 nm drops by 76% for 1PA, the 2PA ESA signal drops only by 27%, providing compelling evidence that **ADA** follows different relaxation pathways after 1PA and 2PA.

The different excited-state dynamics for **ADA**, under 1PA and 2PA, are observed in both DCM and CHX (see Figures S1B and S2) thus suggesting that solvent effects do not govern the 2PA excited-state dynamics. Instead, the 2PA decay appears to be a fundamental property of the molecular framework. To elucidate its origin, we carried out TD-DFT single-point scans as a function of the two dihedral angles linking pyrrolo-pyrrole core with *C*-substituents located at positions 2 and 5 and *N*-substituents located at positions 1 and 4 (denoted as CN- and Ph-dihedral, respectively) based on the optimized ground-state geometry of **ADA** (Figure 3A and 3B, respectively). We find, in agreement with the optimized S_1 structure, that the CN-dihedral is reduced to enhance conjugation along the **ADA** molecular axis thereby lowering the state in energy. Furthermore, we observe that the energy of the S_1 state is independent of the Ph-dihedral angle in the Franck-Condon region, in agreement with no change in this coordinate between the optimized S_1 and S_0 structures (Figure 3B, singlet states). The initial S_1 decay is thus only governed by the CN-dihedral (bond-length changes in coordinates expected for a ππ* transition that were not calculated). In contrast, the 2PA excited S_3 state shows no dependence on either angle and is almost degenerate in energy to the S_2 state. In light of the energetic proximity, it is reasonable to assume that S_3 rapidly decays to S_2 within the time-resolution of our fs-TA experiment (<150 fs). In S_2, we retrieve a similar dependence on the CN-dihedral, as for S_1, towards planarization. Surprisingly, the S_2 state also displays a large gradient of the Ph-dihedral angle, favoring planarization along the orthogonal **ADA** molecular axis (Figure 3B, singlet states). The 2PA excited-state decay is thus likely determined by the interplay of the two perpendicular planarization coordinates, which energetically oppose each other due to steric interactions.

We carried out the same single-point calculations for the triplet manifold of **ADA** (Figures 3A and 3B, triplet states) to investigate

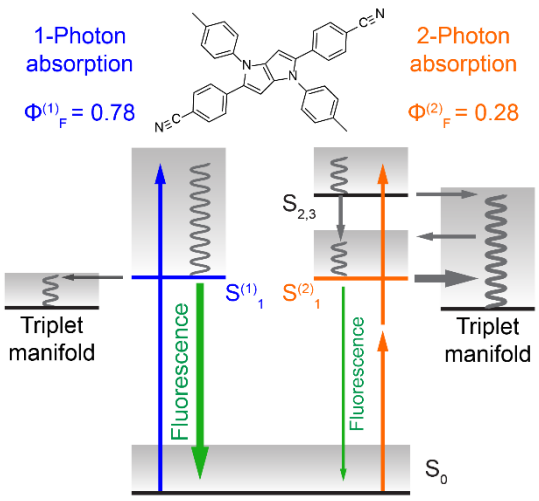

Figure 4. Excited-state dynamics of **ADA** after 1PA and 2PA. The **ADA** molecules can access different fluorescent states $S^{(1)}_1$ and $S^{(2)}_1$ after 1PA and 2PA, leading to different fluorescence quantum yield ($\Phi^{(1)}_F$ and $\Phi^{(2)}_F$), respectively. The difference likely results from unique molecular conformation change in the hot excited-states.

the density of triplet states as a function of their dihedral angle dependence. We find that only one triplet state is reasonably proximate in energy to S_1, while we observe a drastically enhanced density of triplet states around the 2PA excited-state energy. Furthermore, the triplet states (T_3 to T_5, Figure 3B, triplet states) exhibit similar behavior as a function of the dihedral angle as for S_2, suggesting that fast and efficient intersystem crossing from S_3/S_2 to the triplet manifold can promote decay following 2PA, ultimately resulting in an altered branching ratio into S_1 and T_2 compared to 1PA.

Our computational results provide compelling evidence for the notion that the S_1 state, formed upon 2PA, is different in configuration along the Ph-dihedral coordinate as compared to 1PA excitation. This interpretation necessitates the presence of a rotational energetic barrier between the two proposed emissive conformers to avoid thermalization to a common S_1 state. Commonly, such rotational barriers are located at dihedral angles of 0 or 90 degrees relative to the donor core unit of **ADA,** which we cannot accurately describe within a TD-DFT framework. We note that multi-configurational computational studies are needed to obtain the complete potential energy surfaces of **ADA** along the key nuclear displacements; such intricate computational examination constitutes a separate study.

While the experimental data fits a serial model, the calculations suggest that a more convoluted decay pathway may be operative at the earliest times (<150 fs), in which the initially photoexcited S_3 state either branches directly to the triplet manifold or undergoes internal conversion via S_2 prior to intersystem crossing to T_6. It is furthermore possible that re-intersystem crossing from a higher lying triplet state leads to population of the S_1 state. The possibility of a complex interplay of different ultrafast decay channels involving the triplet manifold and different spin-orbital couplings (Figure 3), is most likely the cause for the formation of a different S_1 state. Examination of the natural transition orbitals (NTOs) for all states shown in Figure 3 further suggests that these relaxation pathways strongly involve the pyrrole-N-bound phenyl moiety of **ADA** (Figure S5B). Combined with our experimental observations of Figures 1 and 2, we ascribe the structural origin for the observed 2PA dynamics to be due to population of S_1 on a different configurational space on its potential energy surface, one that involves the phenyl pyrrolo-pyrrole dihedral angle, which is not manifested in the 1PA.

From the results of time-resolved fluorescence, transient absorption spectroscopy and TD-DFT calculations, we may rationalize the excited-state dynamics of **ADA** (Figure 4). Following 1PA to S_1, the excited molecules may relax via fluorescence deactivation with minor intersystem crossing to the triplet state manifold. In contrast, population of S_1 via 2PA occurs via dynamic relaxation through the S_3 to S_2 states and then rapid internal conversion to S_1 on a different local minimum (indicated by $S^{(2)}_1$ vs population of $S^{(1)}_1$ via 1PA). If 2PA would lead to the same molecular configuration on S_1 as for 1PA, we would expect identical fluorescence spectral profiles, transient absorption spectra, and transient decay kinetics in stark contrast to our observations (see Figures 1B and 2). **ADA** must consequently undergo critical changes during its decay after 2PA. Indeed, the TD-DFT simulations show that the S_2 state can induce significant changes in the Ph-dihedral (perpendicular to the **ADA** axis) towards a smaller angle (Figure 3). Importantly, the S_1 state has a flat potential surface with respective to the Ph-dihedral angle. The smaller Ph-dihedral angle induced on S_2 state thus likely persist on the S_1 state and hence generates the different S_1 state compared to 1PA. When noting the density of triplet states lying close to the S_3 and S_2 (see Figure 3), another possible pathway includes molecules on S_3 or S_2 undergoing fast intersystem crossing to the triple state manifold, where the molecular structure subtly changes in a similar manner. To form the fluorescent emissive state, the molecules must return to a different S_1 state through another intersystem crossing, otherwise, no fluorescence could be observed. We note that our results can also be rationalized as a photoselection effect whereby different ground-state populations are photoexcited and subsequently locked in place on the excited state manifold, preventing thermalization on the S_1 surface. Further calculations are required to completely entangle the precise decay pathways.

Different S_1 states lead to distinct excited-state dynamics. As observed in Figure 2E for 1PA, after cooling and solvation, the S_1 signal (blue line) at 550 nm drops by 76% to the long-lived triplet state (green line) due to fluorescence. This is consistent with the 0.78 fluorescence quantum yield measurement. The corresponding drop for 2PA is only 27% as shown in Figure 2F. The reduced drop of the 2PA case could result from two different scenarios: (1) The S_1 fluorescence quantum yield for at the different configurations $S^{(1)}_1$ and $S^{(2)}_1$ are similar, but for 2PA excitation, the subsequently produced triplet state exhibits a ~3 fold enhanced ESA coefficient at 550 nm compared to the singlet state ($\varepsilon_T^{(2PA)}/\varepsilon_T^{(1PA)} = 73/24$); (2) The triplet ESA coefficients remain similar for 1PA and 2PA, but the fluorescence quantum yield for the 2PA excitation is lower than that of 1PA excitation ($\eta^{(1PA)}/\eta^{(2PA)} = 76/27$). We propose case (2) because (i) it is unlikely that similar Franck-Condon factors would prevail for different configurations and (ii) the spectral line shapes of the ESA peak is perfectly matched for 1PA and 2PA transient absorption experiments. It is therefore unlikely that the triplet states formed after 2PA display a nearly 3-fold different absorption coefficient (ε_T). The experimental results thus are consistent with a

different configuration in the S_1 state that is accessed by 2PA. Dynamics that engender these different configurations on S_1, and hence different 1PA and 2PA fluorescence quantum yields, will be promoted by the higher conformational degree of freedom along the benzene ring rotation.

We can now estimate the actual fluorescence quantum yield after 2PA based on the ESA signal drop at 550 nm. Assuming the 76% signal drop extracted from the EADS (Figure 2) corresponds to a 1PA fluorescence quantum yield 0.78, the 27% signal drop for 2PA indicates a fluorescence quantum yield of 0.28. Similarly, for **ADA** in CHX (see Figure S3), we estimate the 2PA fluorescence quantum yield to be 0.27 as opposed to its 1PA fluorescence quantum yield of 0.63.[24] This difference is in contradistinction to the often employed assumption that 1PA and 2PA fluorescence quantum yields are identical. Crucially, this assumption is typically used to determine the 2PA cross-sections of the studied chromophore.[36,37,44] Based on our results for **ADA**, we believe that many 2PA cross-sections reported over the last decades may need to be re-evaluated to discount possible distortions leading to fluorescence loss-channels arising from excited state dynamics. This will be particularly critical for quadrupolar, centrosymmetric molecules, such as **ADA**, which are work-horses for 2PA applications. We remark that the reported 2PA cross-sections for **ADA** were not obtained using a well-characterized reference 2PA dye.[24,44] Our results highlight that the emitting states may differ from 2PA reference dyes depending on their excited state dynamics properties. Further studies are needed to establish the generality of this behavior, especially for centro-symmetric, quadrupolar two-photon chromophores.

We have conducted time-resolved fluorescence and broadband femtosecond transient absorption spectroscopy for **ADA** under 1- and 2PA in a polar and a non-polar solvents. We observed a prolonged fluorescent state lifetime accompanied by spectral broadening under 2PA compared to 1PA, suggesting that emission occirs from the S_1 state for both 1PA and 2PA but from different positions on the potential energy surface owing to dynamics; this results in different fluorescence properties of 1PA and 2PA excited molecules. Similarly, transient absorption shows significant differences between 1PA and 2PA excitations, whereby the 1PA fluorescent state is mostly depopulated by fluorescence while the 2PA fluorescence state is depopulated predominantly by intersystem crossing, which we attribute to a different configuration of **ADA** on S_1. Our study highlights the importance of correctly characterizing the nature of the fluorescent state after two- or multiphoton excitation based on spectral characterization and temporal observation of the excited-state dynamics. Furthermore, our results suggest that, depending on the specific application, the optical properties of **ADA** fluorophores could be significantly improved by targeted engineering of the rates for fluorescence and intersystem crossing.

ASSOCIATED CONTENT

Supporting Information

Materials and methods, supplementary figures and discussion of 1-PA and 2PA photodynamics of **ADA** in CHX.

AUTHOR INFORMATION

Corresponding Author

* E-mails: dnocera@fas.harvard.edu; dtgryko@icho.edu.pl

Present Address

† Cavendish Laboratory, University of Cambridge, JJ Th omson Avenue, Cambridge, CB3 0HE, UK

Notes

¥ Authors contributed equally.

The authors declare no competing financial interest.

ACKNOWLEDGMENT

This work was supported by the National Science Foundation under grant CHE-1855531 and the Foundation for Polish Science (POIR.04.04.00-00-3CF4/16-00). We want to thank Dr. Andrew G. Maher and Rui Sun for helpful discussion. The computations in this paper were run on the Odyssey cluster supported by the FAS Division of Science, Research Computing Group at Harvard University.

REFERENCES

(1) Denk, W.; Strickler, J. H.; Webb, W. W. Two-Photon Laser Scanning Fluorescence Microscopy. *Science* **1990,** *248*, 73-76.

(2) Helmchen, F.; Denk, W. Deep Tissue Two-Photon Microscopy. *Nat. Methods* **2005,** *2*, 932-940.

(3) Diaspro, A.; Robello, M. Two-Photon Excitation of Fluorescence for Three-Dimensional Optical Imaging of Biological Structures. *J. Photochem. Photobiol. B: Biol.* **2000,** *55*, 1-8.

(4) Cahalan, M. D.; Parker, I.; Wei, S. H.; Miller, M. J. Two-Photon Tissue Imaging: Seeing the Immune System in a Fresh Light. *Nat. Rev. Immunol.* **2002,** *2*, 872-880.

(5) Benninger, R. K.; Piston, D. W. Two-Photon Excitation Microscopy for the Study of Living Cells and Tissues. *Curr. Protoc. Cell Biol.* **2013,** *4*, 1-24.

(6) Butko, M. T.; Drobizhev, M.; Makarov, N. S.; Rebane, A.; Brinkman, B. C.; Gleeson, J. G. Simultaneous Multiple-Excitation Multiphoton Microscopy Yields Increased Imaging Sensitivity and Specificity. *BMC Biotechnol.* **2011,** *11*, 20.

(7) Therien, M. J. How to Improve Your Image. *Nature* **2009,** *458*, 716-717.

(8) Cumpston, B. H.; Ananthavel, S. P.; Barlow, S.; Dyer, D. L.; Ehrlich, J. E.; Erskine, L. L.; Heikal, A. A.; Kuebler, S. M.; Lee, I. Y. S.; McCord-Maughon, D.; Qin, J. Q.; Rockel, H.; Rumi, M.; Wu, X. L.; Marder, S. R.; Perry, J. W. Two-Photon Polymerization Initiators for Three-Dimensional Optical Data Storage and Microfabrication. *Nature* **1999,** *398*, 51-54.

(9) Walker, E.; Rentzepis, P. M. A New Dimension. *Nat Photonics* **2008,** *2*, 406.

(10) Hayat, A.; Nevet, A.; Ginzburg, P.; Orenstein, M. Applications of Two-Photon Processes in Semiconductor Photonic Devices: Invited Review. *Semicond. Sci. Technol.* **2011,** *26*, 083001.

(11) Bhawalkar, J. D.; Kumar, N. D.; Zhao, C. F.; Prasad, P. N. Two-Photon Photodynamic Therapy. *J. Clin. Laser Med. Surg.* **1997,** *15*, 201-204.

(12) Brown, S. Two Photons Are Better Than One. *Nat Photonics* **2008,** *2*, 394-395.

(13) Collins, H. A.; Khurana, M.; Moriyama, E. H.; Mariampillai, A.; Dahlstedt, E.; Balaz, M.; Kuimova, M. K.; Drobizhev, M.; Yang, V. X. D.; Phillips, D.; Rebane, A.; Wilson, B. C.; Anderson, H. L. Blood-Vessel Closure Using Photosensitizers Engineered for Two-Photon Excitation. *Nat. Photonics* **2008,** *2*, 420-424.

(14) Sui, B. L.; Yue, X. L.; Kim, B.; Belfield, K. D. Near-Ir Two-Photon Fluorescent Sensor for K^+ Imaging in Live Cells. *ACS Appl. Mater. Interfaces* **2015,** *7*, 17565-17568.

(15) Pawlicki, M.; Collins, H. A.; Denning, R. G.; Anderson, H. L. Two-Photon Absorption and the Design of Two-Photon Dyes. *Angew. Chem. Int. Ed.* **2009,** *48*, 3244-3266.

(16) Kim, H. M.; Seo, M. S.; Jeon, S. J.; Cho, B. R. Two-Photon Absorption Properties of Hexa-Substituted Benzene Derivatives. Comparison between Dipolar and Octupolar Molecules. *Chem. Commun.* **2009**, 7422-7424.

(17) He, G. S.; Tan, L. S.; Zheng, Q.; Prasad, P. N. Multiphoton Absorbing Materials: Molecular Designs, Characterizations, and Applications. *Chem. Rev.* **2008,** *108*, 1245-1330.

(18) Janiga, A.; Glodkowska-Mrowka, E.; Stoklosa, T.; Gryko, D. T. Synthesis and Optical Properties of Tetraaryl-1,4-Dihydropyrrolo-[3,2-B]Pyrroles. *Asian J. Org. Chem.* **2013,** *2*, 411-415.

(19) Krzeszewski, M.; Thorsted, B.; Brewer, J.; Gryko, D. T. Tetraaryl-, Pentaaryl-, and Hexaaryl-1,4-Dihydropyrrolo[3,2-B]Pyrroles: Synthesis and Optical Properties. *J. Org. Chem.* **2014,** *79*, 3119-3128.

(20) Janiga, A.; Gryko, D. T. 1,4-Dihydropyrrolo[3,2-B]Pyrrole and Its Pi-Expanded Analogues. *Chem. Asian J.* **2014,** *9*, 3036-3045.

(21) Janiga, A.; Krzeszewski, M.; Gryko, D. T. Diindolo[2,3-B:2 ',3'-F]Pyrrolo[3,2-B]Pyrroles as Electron-Rich, Ladder-Type Fluorophores: Synthesis and Optical Properties. *Chem. Asian J.* **2015,** *10*, 212-218.

(22) Krzeszewski, M.; Gryko, D.; Gryko, D. T. The Tetraarylpyrrolo[3,2-B]Pyrroles-from Serendipitous Discovery to Promising Heterocyclic Optoelectronic Materials. *Acc. Chem. Res.* **2017,** *50*, 2334-2345.

(23) Janiga, A.; Bednarska, D.; Thorsted, B.; Brewer, J.; Gryko, D. T. Quadrupolar, Emission-Tunable Pi-Expanded 1,4-Dihydropyrrolo[3,2-B]Pyrroles - Synthesis and Optical Properties. *Org. Biomol. Chem.* **2014,** *12*, 2874-2881.

(24) Friese, D. H.; Mikhaylov, A.; Krzeszewski, M.; Poronik, Y. M.; Rebane, A.; Ruud, K.; Gryko, D. T. Pyrrolo[3,2-B]Pyrroles-from Unprecedented Solvatofluorochromism to Two-Photon Absorption. *Chem. Eur. J.* **2015,** *21*, 18364-18374.

(25) Dereka, B.; Rosspeintner, A.; Krzeszewski, M.; Gryko, D. T.; Vauthey, E. Symmetry-Breaking Charge Transfer and Hydrogen Bonding: Toward Asymmetrical Photochemistry. *Angew. Chem. Int. Ed.* **2016,** *55*, 15624-15628.

(26) Dereka, B.; Rosspeintner, A.; Stezycki, R.; Ruckebusch, C.; Gryko, D. T.; Vauthey, E. Excited-State Symmetry Breaking in a Quadrupolar Molecule Visualized in Time and Space. *J. Phys. Chem. Lett.* **2017,** *8*, 6029-6034.

(27) Terenziani, F.; Painelli, A.; Katan, C.; Charlot, M.; Blanchard-Desce, M. Charge Instability in Quadrupolar Chromophores: Symmetry Breaking and Solvatochromism. *J. Am. Chem. Soc.* **2006,** *128*, 15742-15755.

(28) Dereka, B.; Vauthey, E. Solute-Solvent Interactions and Excited-State Symmetry Breaking: Beyond the Dipole-Dipole and the Hydrogen-Bond Interactions. *J. Phys. Chem. Lett.* **2017,** *8*, 3927-3932.

(29) Ivanov, A. I.; Dereka, B.; Vauthey, E. A Simple Model of Solvent-Induced Symmetry-Breaking Charge Transfer in Excited Quadrupolar Molecules. *J. Chem. Phys.* **2017,** *146*, 164306.

(30) Lemon, C. M.; Karnas, E.; Bawendi, M. G.; Nocera, D. G. Two-Photon Oxygen Sensing with Quantum Dot-Porphyrin Conjugates. *Inorg. Chem.* **2013,** *52*, 10394-10406.

(31) Lemon, C. M.; Karnas, E.; Han, X. X.; Bruns, O. T.; Kempa, T. J.; Fukumura, D.; Bawendi, M. G.; Jain, R. K.; Duda, D. G.; Nocera, D. G. Micelle-Encapsulated Quantum Dot-Porphyrin Assemblies as in Vivo Two-Photon Oxygen Sensors. *J. Am. Chem. Soc.* **2015,** *137*, 9832-9842.

(32) De Wergifosse, M.; Houk, A. L.; Krylov, A. I.; Elles, C. G. Two-Photon Absorption Spectroscopy of Trans-Stilbene, Cis-Stilbene, and Phenanthrene: Theory and Experiment. *J. Chem. Phys.* **2017,** *146*, 144305.

(33) Schalk, O.; Boguslavskiy, A. E.; Stolow, A. Two-Photon Excited State Dynamics of Dark Valence, Rydberg, and Superexcited States in 1,3-Butadiene. *J. Phys. Chem. Lett.* **2014,** *5*, 560-565.

(34) Moreno, J.; Dobryakov, A. L.; Ioffe, I. N.; Granovsky, A. A.; Hecht, S.; Kovalenko, S. A. Broadband Transient Absorption Spectroscopy with 1- and 2-Photon Excitations: Relaxation Paths and Cross Sections of a Triphenylamine Dye in Solution. *J. Chem. Phys.* **2015,** *143*, 024311.

(35) Maus, M.; Rettig, W.; Bonafoux, D.; Lapouyade, R. Photoinduced Intramolecular Charge Transfer in a Series of Differently Twisted Donor - Acceptor Biphenyls as Revealed by Fluorescence. *J. Phys. Chem. A* **1999,** *103*, 3388-3401.

(36) Xu, C.; Webb, W. W. Measurement of Two-Photon Excitation Cross Sections of Molecular Fluorophores with Data from 690 to 1050 nm. *J. Opt. Soc. Am. B* **1996,** *13*, 481-491.

(37) Rumi, M.; Perry, J. W. Two-Photon Absorption: An Overview of Measurements and Principles. *Adv. Opt. Photonics* **2010,** *2*, 451-518.

(38) Braem, O.; Penfold, T. J.; Cannizzo, A.; Chergui, M. A Femtosecond Fluorescence Study of Vibrational Relaxation and Cooling Dynamics of UV Dyes. *Phys. Chem. Chem. Phys.* **2012,** *14*, 3513-3519.

(39) Reynolds, L.; Gardecki, J. A.; Frankland, S. J. V.; Horng, M. L.; Maroncelli, M. Dipole Solvation in Nondipolar Solvents: Experimental Studies of Reorganization Energies and Solvation Dynamics. *J. Phys. Chem.* **1996,** *100* (24), 10337-10354.

(40) Maroncelli, M.; Fleming, G. R. Picosecond Solvation Dynamics of Coumarin-153 - the Importance of Molecular Aspects of Solvation. *J. Chem. Phys.* **1987,** *86*, 6221-6239.

(41) Bagchi, B.; Jana, B. Solvation Dynamics in Dipolar Liquids. *Chem. Soc. Rev.* **2010,** *39*, 1936-1954.

(42) Qin, Y.; Chang, C. W.; Wang, L.; Zhong, D. Validation of Response Function Construction and Probing Heterogeneous Protein Hydration by Intrinsic Tryptophan. *J. Phys. Chem. B* **2012,** *116*, 13320-13330.

(43) Dorlhiac, G. F.; Fare, C.; van Thor, J. J. Pyldm - an Open Source Package for Lifetime Density Analysis of Time-Resolved Spectroscopic Data. *PLoS Comput. Biol.* **2017,** *13*, e1005528.

(44) Makarov, N. S.; Drobizhev, M.; Rebane, A. Two-Photon Absorption Standards in the 550-1600 nm Excitation Wavelength Range. *Opt. Express* **2008,** *16*, 4029-4047.

Supporting Information

Direct Observation of Different One- and Two-Photon Fluorescent States in a Pyrrolo[3,2-b]Pyrrole Fluorophore

Yangzhong Qin,[a] Christoph Schnedermann,[a] Mariusz Tasior,[b] Daniel T. Gryko*,[b] and Daniel G. Nocera*,[a]

[a] *Department of Chemistry and Chemical Biology, Harvard University, 12 Oxford Street, Cambridge, MA 02138, United States.* [b] *Institute of Organic Chemistry, Polish Academy of Sciences, Kasprzaka 44/52, 01-224 Warsaw, Poland.*

* dnocera@fas.harvard.edu

*dtgryko@icho.edu.pl

Table of Contents

Materials and Methods

Sample Preparation. **ADA** was synthesized according the published procedure.[1] The purified sample was dissolved in either dichloromethane (DCM) or cyclohexane (CHX) in aerobic condition at room temperature. UV-vis spectra were measured with a Varian Cary 5000 UV-vis-NIR spectrometer. For spectroscopic measurements, the samples were filtered (0.2 μm PTFE filter) and diluted to concentration of ~15 μM and ~5 μM in DCM and CHX, respectively.

Steady-State Emission Measurements. The steady-state emission spectra were measured by a Photon Technology International (PTI) QM4 fluorimeter equipped with a 150 W Xe arc lamp as excitation light source and a dry ice cooled photomultiplier tube (PMT) as the detection unit. Samples were contained in a 1-cm quartz cuvette. The OD at the excitation wavelength of 360 nm was 0.11 for CHX samples and 0.278 for DCM samples.

Time-Resolved Fluorescence Spectroscopy. Time-resolved fluorescence emission was collected using a Hamamatsu C4334 Streak Scope camera[2] at 90 degrees with a pump at either 360 nm or 720 nm provided by a femtosecond noncollinear optical parametric amplifier (see femtosecond transient absorption setup section for more details). The pump pulse energy was set to 60 nJ and 25 μJ for excitation at 360 nm and 720 nm, respectively. The excitation beam has a diameter of ~600 μm at its full-width-half-maximum. The samples were the same as used in the steady-state emission measurement and stored in a 1-cm quartz cuvette (OD ~ 0.11 and 0.278 (λ_{exc} = 360 nm) for **ADA** in CHX and DCM, respectively). The obtained spectral intensities were not corrected for the wavelength-dependent collection efficiency of the respective setups, but the experiments were conducted under the same conditions such that a direct comparison of the spectra after 1PA and 2PA is not affected. The detected fluorescence signal followed a linear power dependence in 1PA and a square power dependence in 2PA.

The time-resolved emission decay (Figure 1B and Figure S1B) was fitted with a single exponential function convoluted with the instrument response function (IRF), showing as the following:

$$S = e^{-\frac{t}{\tau}} \otimes IRF + baseline$$

where, t is time, τ is the exponential decay time constant, IRF is a Gaussian function with full width half maxim (FWHM), and a possible baseline,

$$G(FWHM, t) = \frac{2\sqrt{\ln(2)}}{\sqrt{\pi} \times FWHM} \times \exp\left(-\left[\frac{2\sqrt{\ln(2)} \times t}{FWHM}\right]^2\right)$$

The overall signal can be written as the following:

$$S = Ae^{\left[\left(\frac{FWHM}{\sqrt{2}\times 2\sqrt{2\ln(2)}\times\tau}\right)^2 - \frac{t}{\tau}\right]} \times erfc\left(\frac{FWHM}{\sqrt{2} \times 2\sqrt{2\ln(2)} \times \tau} - \frac{t \times 2\sqrt{2\ln(2)}}{\sqrt{2} \times FWHM}\right) + baseline$$

A is an amplitude factor and erfc is the complementary error function. As shown in Figures 1B and S1B, the baseline is negligible in the fitting. FWHM was determined to be 450 ps, by fitting the light scattering near the excitation wavelength while using pure solvent.

Estimation of Self-Absorption Effects for Time-Resolved Emission Spectra. Self-absorption is commonly observed for samples with overlapped absorption and emission spectra. This effect will change the emission spectrum if the sample is strongly absorbing. We note that this is not the case for the study here. At the excitation wavelength of 360 nm, the absorbance of the sample in cyclohexane is 0.11 and in DCM the absorbance is 0.278. We use Cormier's analysis[3] to determine perturbations introduced by self-absorption. The cyclohexane sample, with an excitation absorbance of 0.11, shows no discernible self-absorption. Thus we report only on **ADA** in DCM.

We analyze the self-absorption effect and correct the emission spectrum for the most extreme condition, where 1PA is exciting the solution at the incident surface due to the "strong" absorption, and 2PA is exciting the solution at the center of the 1-cm cuvette due to the weak absorption, and the focusing position at the center of the cuvette (see Figure S2A). To have the largest difference for self-absorption between 1PA and 2PA, we use optical path length (L) of L_{1PA}= 0.71 cm and L_{2PA}= 0.5 cm (see Figure S2A). Note that this case does not apply to ADA in DCM as the 1PA absorbance at 360 nm is 0.278; with a 1 cm pathlength, this optical density (OD) corresponds to a total absorption of 47% of the incident light; thus the excitation volume under 1PA is definitely not at the surface of the cuvette. Nonetheless, we will apply the most extreme analysis conditions, shown in Figure S2A to **ADA** in DCM and the following correction will over-estimate the self-absorption effect.

Cormier's analysis[3] begins by relating the intensity of the emission spectrum to Beer's Law,

$$I_0(\lambda) = I(\lambda)10^{\varepsilon(\lambda)cL}$$

where $I_0(\lambda)$ is the emission intensity from the excitation volume (the true emission intensity), $I(\lambda)$ is the directly measured emission intensity with self-absorption effect, $\varepsilon(\lambda)$ is the molar extinction coefficient, c is the concentration, and $L(\lambda)$ is the optical path length. Therefore, for 1PA,

$$I_{0,1PA}(\lambda) = I_{1PA}(\lambda)10^{\varepsilon(\lambda)cL_{1PA}}$$

and for 2PA,

$$I_{0,2PA}(\lambda) = I_{2PA}(\lambda)10^{\varepsilon(\lambda)cL_{2PA}}$$

The corrected and uncorrected emission spectra for **ADA** in DCM is plotted in Figure S2B. We note that the correction is manifest only at the blue edge of the emission, in the 0,0 transition regime where the absorption and emission spectra would overlap. At longer wavelengths, self-absorption is absent. Indeed, for the concentrations of **ADA** used in DCM, self-absorption is

minimal at wavelengths greater than 443 nm as the absorbance is less than 0.1. These results suggest that the differences between 1 PA and 2PA spectra, namely the broadening of the 2PA spectrum relative to the 1PA spectrum, is not due to self-absorption.

Nanosecond Transient Absorption Spectroscopy. The nanosecond time-resolved transient absorption spectroscopy setup was previously reported.[4] Briefly, a pump pulse was generated by a Quanta-Ray Nd:YAG laser (SpectraPhysics) providing 3rd harmonic at 355 nm with a repetition rate of 10 Hz and pulse width of ~10 ns (FWHM). The pump pulse energy was set to ~0.4 mJ and beam size is ~2 mm in diameter. Probe light was generated by a 75 W Xe-arc lamp and partially selected by a 2 mm diameter pinhole. Both pump and probe were focused and overlapped on the sample with ~15° angle. The sample was flowed through a 1 cm path-length flow cell (Starna Cells) to prevent sample damage. Single-wavelength transient absorption traces were detected by a PMT and recorded by a 1 GHz oscilloscope (LeCroy 9384CM).

Broadband Femtosecond Transient Absorption Spectroscopy. The broadband femtosecond transient absorption setup is based on a previously reported single-shot probe-referenced transient absorption design.[5] A Ti:Sapphire regenerative amplifier (Coherent Libra-HE) provides 3 W fundamental pulses (800 nm, ~50 fs) at 1 kHz. An OPerA SOLO (Coherent) is seeded with 2 W of the fundamental to provide pump pulses at 720 and 360 nm. The pump pulses were subsequently aligned onto a 1.7 m computer-controlled, motorized translation stage (Aerotech ATS62150, U100 controller) equipped with a hollow retro-reflector (Newport) followed by an ultrabroadband polarizer and λ/2 waveplate (Thorlabs) to produce linearly polarized pulses at magic angle with respect to the probe pulse. The pulse duration at the sample for the 720 nm pump pulse was determined to be ~60 fs based on frequency-resolved optical gating.[6] The 360 nm pump pulse has a duration of ~120 fs based on the bleach rise time in our 1PA transient absorption experiments. We thus conservatively estimate a time-resolution of <150 fs in our experiments. The pulse energy was set to 60 nJ and 1 μJ for pump pulses at 360 and 720 nm, respectively. The detected transient absorption signals were verified to follow a linear power dependence in 1PA and a square power dependence in 2PA.

Chirped white light pulses were generated by focusing a fraction (~1 mW) of the remaining laser output (f = 100 mm, Thorlabs) into a 5 mm calcium fluoride (CaF_2) that was continuously translated back-and-forth perpendicular to the input beam to avoid thermal damage. The generated pulses were reflectively collimated (f = 50 mm, Thorlabs) and aligned onto a 15 mm translation stage (PhysikInstrumente, M-111.DG, Mercury DC controller). A notch filter (EKSMA, VEI6053) removed the residual fundamental and the white light pulses were subsequently sent onto a broadband reflective neutral density filter (Thorlabs, NDUV04B) to generate probe (reflected) and reference (transmitted) pulses of approximately equal intensity.[4] The setup was tested to be shot-noise limited down to 1 μOD.

Pump, probe and reference pulses were reflectively focused into the sample (f = 200 mm) to yield Gaussian beams with diameters (full-width-half-maximum) of 70 μm (pump) and 40 μm

(probe/reference). The transmitted probe and reference pulses were subsequently collimated reflectively (f = 200 mm) before being send into a home-build fused-silica prism (OptoSigma, DPSQ-20-10H) spectrograph (f = 250 mm) equipped with two 16 bit, 512 pixel charge-coupled devices (Hamamatsu S7030-0906). Data acquisition was enabled by a custom-build interface board from Entwicklungsbüro Stresing. Differential normalized transmittance signals were collected on shot-to-shot basis with the pump chopped at 500 Hz.

The same home-build sample cell was used for all experiments with a path-length of 500 μm adjusted by Teflon spaces mounted between two BK7 round cover-glasses (thickness ~110 μm). The sample was flowed through the cell in a gravity-driven configuration to reduce peristaltic pump-induced signal fluctuations.[7] The **ADA** concentrations were ~200 μM and ~50 μM in DCM and CHX, respectively, but because of the smaller pathlength, optical densities are significantly lower than that of the samples used in the steady-state emission and the time-resolved emission measurements.

A single transient absorption trace consisted of 200 collected probe shots, resulting in 100 differential spectra, which were averaged for each time point. Data presented in this study was obtained by recording 60 transient absorption traces and averaging the results. Long data sets (>3 ps) were recorded by temporally adjusting the pump pulse, while short data sets (<3 ps) were recorded by probe-translation for higher temporal accuracy. Both datasets were combined in Figures 2 and S2 and subtracted for the solvent response under identical experimental conditions.

Computational Methods. Quantum-chemical calculations were performed with Gaussian 16[8] using density-functional theory (DFT). Tight geometry optimizations were carried out at the MN15/def2-TZVP level of theory including a continuum polarizable continuum model (cPCM) for the solvent (DCM), which accurately reproduces the structure of **ADA** based on crystallographic and computational results.[8] Frequency calculations verified the optimized structure (no negative frequencies). To speed up calculations marginally, we replaced the methyl substituent on the N-bound phenyl groups with Hydrogen atoms. The corresponding frontier molecular orbitals are illustrated in Figure S5A.

Time-dependent DFT at the same level of theory calculated the lowest 15 singlets and triplet states and was used to generate natural transition orbitals (NTOs) for the lowest three singlet states (Figure S5B). In agreement with previous gas-phase calculations on a reduced **ADA** molecule, the first two singlet transitions correspond to optically allowed transition from HOMO → LUMO and HOMO–1 → LUMO (Figure S5B, blue), while the third excited singlet state can be assigned to the optically forbidden, but two-photon absorption allowed transition HOMO → LUMO+1 (Figure S5B, orange). To choose a proper functional to correctly assess the photochemical properties of molecules, we verified that the MN15 functional in combination with the cPCM model compares well with previous studies[9] both in terms of ground state and excited state properties and adequately reproduces the crystal structure of ADA. Together these results suggest that the choice of the MN15 functional is appropriate for our work.

Steady State Emission Spectra

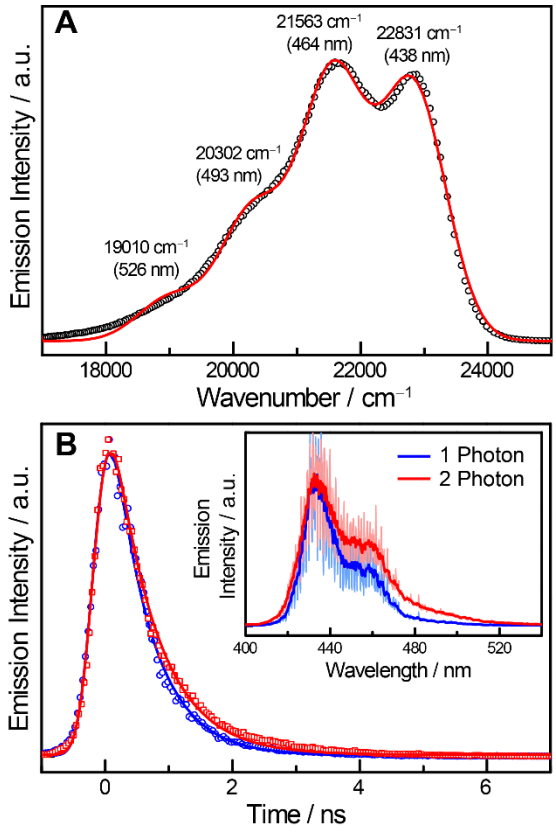

Figure S1. A Steady state emission spectrum of ADA in CHX (black circles) and a fit (red line) with 4 gaussian functions with same width. The peak position of each gaussian component was labelled accordingly. **B** Time-resolved fluorescence decay integrated from 420 to 520 nm of ADA in CHX after 1PA (360 nm, blue) and 2PA (720 nm, red). Solid lines indicate single-exponential model fittings with a lifetime of 590 ps for 1PA (blue) and 670 ps for 2PA (red). The time-integrated fluorescence spectrum is shown in the inset. The raw data (opaque) is also shown and was smoothed by 5-point moving average. The different spectrum profile compared to the steady-state fluorescence spectrum (Figure 1A in the main context) is due to calibration differences but does not affect our comparison (see previous time-resolved fluorescence spectroscopy).

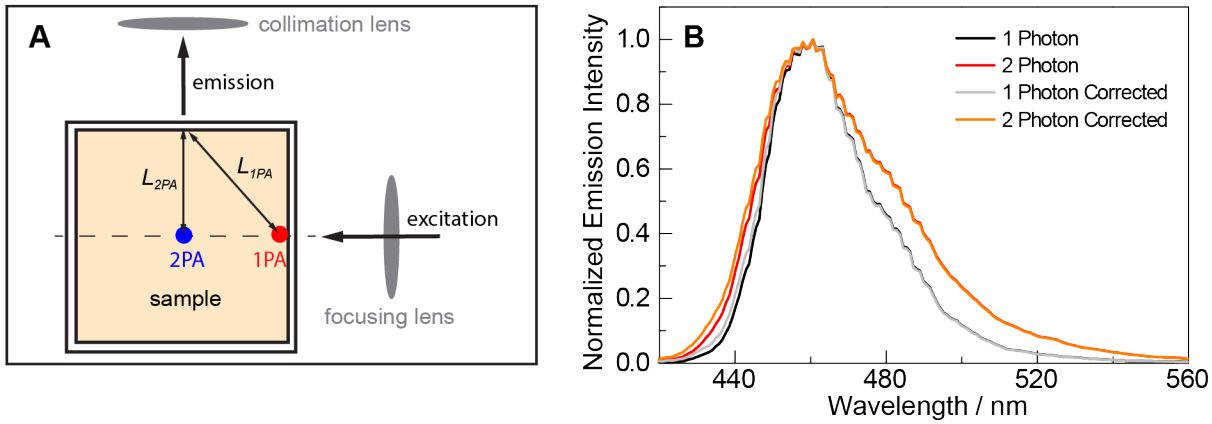

Figure S2. Estimation of self-absorption effect to the observed difference of emission spectra under 1PA and 2PA conditions. **A** Scheme showing an extreme condition with strong inner-filter effect for 1PA and no inner-filter effect for 2PA (see spectrum correction method). The colored circles show the excitation volume in the solution. **B** Corrected and uncorrected emission spectra (see above) for **ADA** in DCM under 1PA and 2PA conditions. The self-absorption only slightly deceases the emission intensity at the blue side shorter than 450 nm. The difference of the emission spectra under 1PA and 2PA remain similar before and after correction.

Broadband Femtosecond Transient Absorption Spectroscopy of ADA in CHX

Figure S3A and S3B show the broadband transient absorption spectra for ADA in CHX after 1PA (360 nm) and two 2PA (720 nm), respectively. The overall transient absorption signal is weaker than that observed in DCM due to limited solubility of ADA in CHX. The excited-state absorption (ESA), the stimulated emission (SE) and the ground-state bleaching (GB) were also similar to that observed in DCM. Figure S3C and S3D show the time evolution of the transient absorption signal observed at selected wavelengths for ADA after 1- and 2PA, respectively. The initial signal rises in ~1 ps and ~20 ps are due to cooling and solvation. As observed for ADA in DCM, all signals dropped over 60% after 1PA within 1 ns. After 2PA, the ESA and SE signal drops marginally, but the GB remains constant. We globally fitted the broadband transient absorption spectra (Figure S3A and S3B) with a serial A→B→C→D→ model for the 1PA and a serial A→B→C→ model for 2PA. The fitted results are illustrated by the solid lines in Figure S3C and S3D and the evolution-associated difference absorption spectra (EADS) are shown in Figure S3E and S3F. The corresponding fitting results for 1PA match previous reports.[10]

For 2PA, we do not observe obvious initial fast transient response within 1 ps (note the constant signal in the first 2 ps in Figure S3D), allowing us to only fit three components to adequately describe the data. We fixed the longest decay constant (670 ps from the fluorescence decay fitting in Figure S1) to achieve the best fitting quality as shown in Figure S3E and S3F. Generally, we observed similar excited-state dynamics for ADA in CHX and DCM. Following 1PA, the fluorescent excited state is predominantly depopulated due to fluorescence and intersystem crossing is minor, while following 2PA, this trend is reversed.

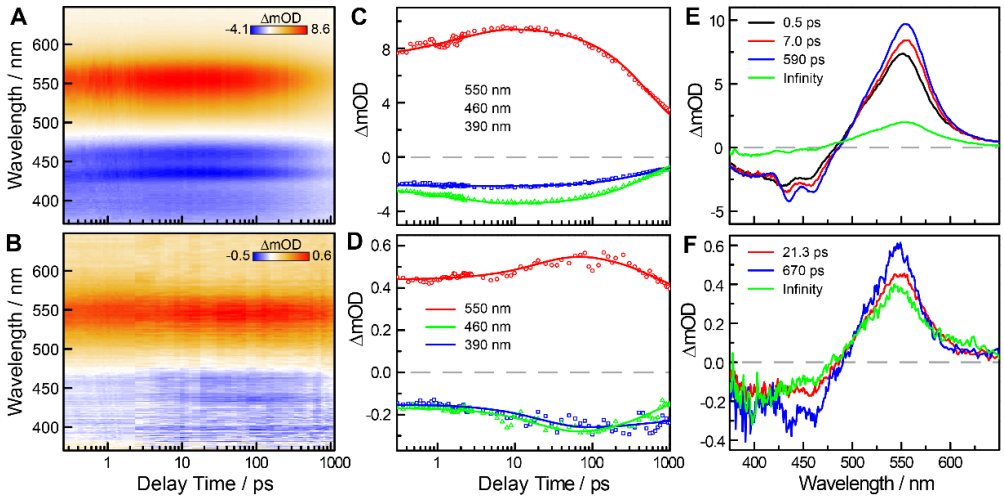

Figure S3. Femtosecond transient absorption spectroscopy of ADA in CHX. Broadband transient absorption spectra of ADA in CHX after **A** 1PA at 360 nm and **B** 2PA at 720 nm. Temporal evolution of representative transients characterizing the ESA (550 nm, red), SE (460 nm, green) and GB (390 nm, blue) for ADA after **C** 1PA and **D** 2PA. Solid lines show a global fit (A→B→C→D→ or A→B→C→ model). Retrieved evolution-assisted decay spectra for **E** 1PA and **F** 2PA. Associated time constants are indicated in the legend.

Nanosecond Transient Absorption Spectra

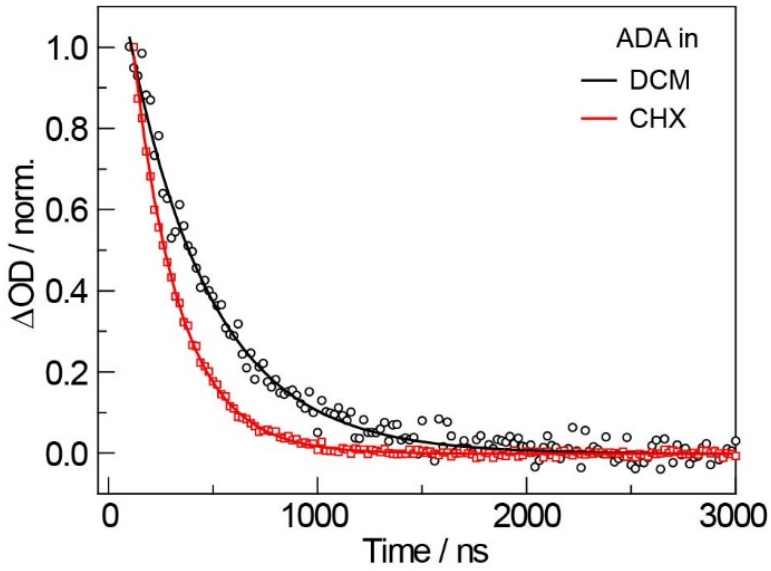

Figure S4. Nanosecond transient absorption at 560 nm for ADA in DCM (black) and CHX (red). Solid lines show single-exponential fits and the corresponding fitted lifetimes (τ) are 390 ns and 220 ns for ADA in DCM and CHX, respectively.

Computational Results

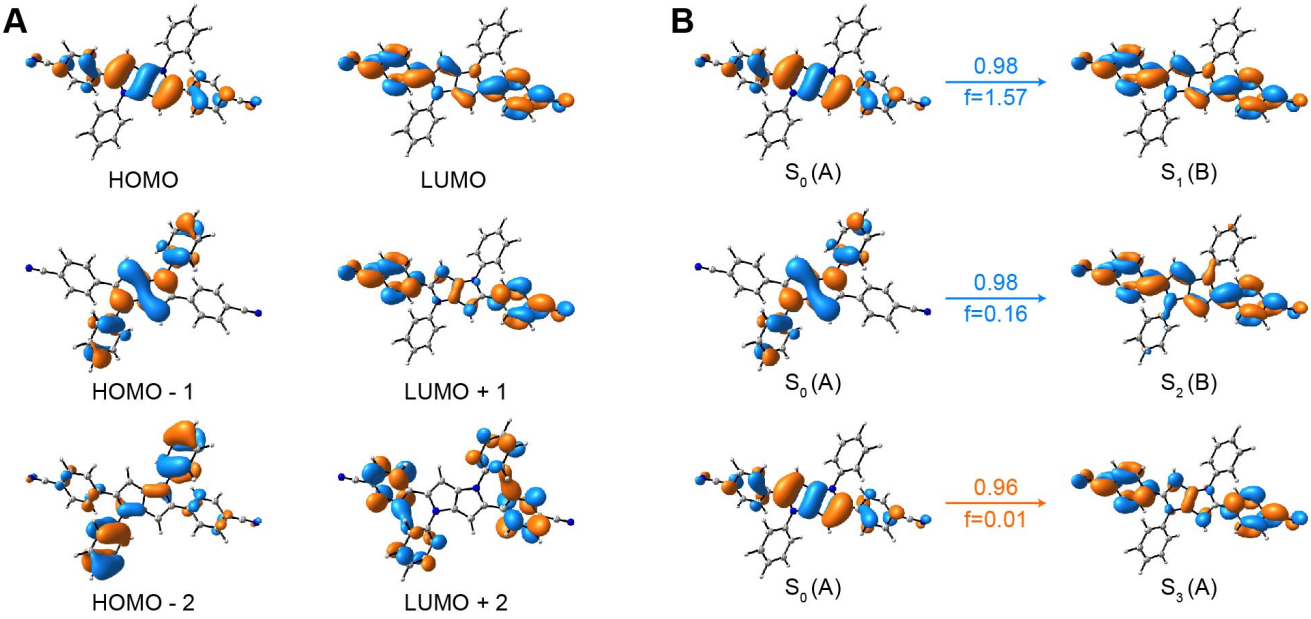

Figure S5. Computational overview of relevant orbitals and transition orbitals. **A** 3 highest energy occupied and lowest unoccupied molecular orbitals (HOMO, LUMO). **B** Natural transition orbitals for transitions to the first three excited singlet state. Symmetries of the displayed orbitals are indicated. Contribution probabilities for the transitions are given, as well as the (1PA) oscillator strengths. Blue denotes one-photon allowed transitions, while orange refers to two-photon allowed transitions based on symmetry.

Reference

(1) Janiga, A.; Glodkowska-Mrowka, E.; Stoklosa, T.; Gryko, D. T. Synthesis and Optical Properties of Tetraaryl-1,4-Dihydropyrrolo-[3,2-B]Pyrroles. *Asian J. Org. Chem.* **2013**, *2*, 411–415.

(2) Loh, Z. H.; Miller, S. E.; Chang, C. J.; Carpenter, S. D.; Nocera, D. G. Excited-State Dynamics of Cofacial Pacman Porphyrins. *J. Phys. Chem. A* **2002**, *106*, 11700–11708.

(3) Cormier, J.-F.; Fortin, M.; Frechette, J.; Noiseux, I.; Vernon, M. L.; Long, W. The Effects of Self-Absorption and detection Geometry on Fluorescence Intensity and Decay Lifetime. *Proc. SPIE* **2005**, 5702, 123–134.

(4) Holder, P. G.; Pizano, A. A.; Anderson, B. L.; Stubbe, J.; Nocera, D. G. Deciphering Radical Transport in the Large Subunit of Class I Ribonucleotide Reductase. *J. Am. Chem. Soc.* **2012**, *134*, 1172–1180.

(5) Bradler, M.; Riedle, E. Temporal and Spectral Correlations in Bulk Continua and Improved Use in Transient Spectroscopy. *J. Opt. Soc. Am. B* **2014**, *31*, 1465–1475.

(6) Trebino, R.; DeLong, K. W.; Fittinghoff, D. N.; Sweetser, J. N.; Krumbugel, M. A.; Richman, B. A.; Kane, D. J. Measuring Ultrashort Laser Pulses in the Time-Frequency Domain Using Frequency-Resolved Optical Gating. *Rev. Sci. Instrum.* **1997**, *68*, 3277–3295.

(7) Kuramochi, H.; Takeuchi, S.; Tahara, T. Femtosecond Time-Resolved Impulsive Stimulated Raman Spectroscopy Using Sub-7-Fs Pulses: Apparatus and Applications. *Rev. Sci. Instrum.* **2016**, *87*, 043107.

(8) Frisch, M. J.; Trucks, G. W.; Schlegel, H. B.; Scuseria, G. E.; Robb, M. A.; Cheeseman, J. R.; Scalmani, G.; Barone, V.; Petersson, G. A.; Nakatsuji, H.; Li, X.; Caricato, M.; Marenich, A. V.; Bloino, J.; Janesko, B. G.; Gomperts, R.; Mennucci, B.; Hratchian, H. P.; Ortiz, J. V.; Izmaylov, A. F.; Sonnenberg, J. L.; D., Williams-Young, Ding, F.; Lipparini, F.; Egidi, F.; Goings, J.; Peng, B.; Petrone, A.; Henderson, T.; Ranasinghe, D.; Zakrzewski, V. G.; Gao, J.; Rega, N.; Zheng, G.; Liang, W.; Hada, M.; Ehara, M.; Toyota, K.; Fukuda, R.; Hasegawa, J.; Ishida, M.; Nakajima, T.; Honda, Y.; Kitao, O.; Nakai, H.; Vreven, T.; Throssell, K.; Montgomery, J. A., Jr.; Peralta, J. E.; Ogliaro, F.; Bearpark, M. J.; Heyd, J. J.; Brothers, E. N.; Kudin, K. N.; Staroverov, V. N.; Keith, T. A.; Kobayashi, R.; Normand, J.; Raghavachari, K.; Rendell, A. P.; Burant, J. C.; Iyengar, S. S.; Tomasi, J.; Cossi, M.; Millam, J. M.; Klene, M.; Adamo, C.; Cammi, R.; Ochterski, J. W.; Martin, R. L.; Morokuma, K.; Farkas, O.; Foresman, J. B.; Fox, D. J. Gaussian 16, Revision B.01; Gaussian, Inc.: Wallingford, CT, 2016.

(9) Friese, D. H.; Mikhaylov, A.; Krzeszewski, M.; Poronik, Y. M.; Rebane, A.; Ruud, K.; Gryko, D. T. Pyrrolo[3,2-B]Pyrroles-from Unprecedented Solvatofluorochromism to Two-Photon Absorption. *Chem. Eur. J.* **2015**, *21*, 18364–18374.

(10) Dereka, B.; Rosspeintner, A.; Krzeszewski, M.; Gryko, D. T.; Vauthey, E. Symmetry-Breaking Charge Transfer and Hydrogen Bonding: Toward Asymmetrical Photochemistry. *Angew. Chem. Int. Ed.* **2016**, *55*, 15624–15628.